

*Journal of Climate Change*, Vol. 9, No. 4 (2023), pp. 53-65. DOI 10.3233/JCC230032

## **Interactions of Seasonal Earth Processes and Climate System**

## Kalman Ziha

University of Zagreb, Department of Naval Architecture and Offshore Engineering, Zagreb − 10000, Croatia ⊠ Kalman.Ziha@fsb.hr

Received September 28, 2023; revised and accepted October 27, 2023

Abstract: The cumulative effects of seasonal Earth processes in different places and times in the atmosphere, hydrosphere, and cryosphere essentially and inevitably shape global climate conditions. Therefore, the article investigates the possibilities for modelling the periodicity of the observable seasonal climate processes. The starting assumption of the study is that the seasonal climate processes are representable by two-phase linear periodic models based on observed data. A numerical algorithm elaborated in the sequel makes it possible to accumulate the seasonal effects of two successively progressive and regressive process phases of periodic climate changes in time. The model first tackles the reported seasonal growth of the atmospheric CO<sub>2</sub> concentration. Next, it considers the observed seasonal cryospheric melting and freezing processes of the Antarctica and Greenland ice sheets and of the Arctic sea ice. It also elaborates on the reported seasonal sea level rise. Finally, the article summarises the interactions of periodic climate processes and the global climate conditions in time scale. The reports on global temperature rise are only on an annual basis. The article also emphasises the importance of control over the seasonal worsening and recovery scenarios for more appropriate projections of climate policies to 2100.

Keywords: Climate; Seasonal; Global; Atmosphere; Hydrosphere, Cryosphere; Policies.

## Introduction

Cumulative Effects Assessments (CEA) of human activities and Earth processes are essential for Environmental Impact Assessments (EIA) of future consequences (Jones, 2016; Roudgarmi, 2018). The properties of two successive phases of seasonally periodic natural processes are often aptly described by peaks of opposite ascriptions like progression and regression, growth and decline, worsening and recovery, increase and decrease, or rise and drop, deterioration and recuperation, etc. The cumulative effects of both phases of dual successive periodic processes largely shape local environmental conditions. There is a lasting empirical lack of physical understanding of the interactions of seasonal and global climate processes. The article implements a heuristic combined numerical and mathematical procedure for the Accumulation of Effects of 2 Phase Periodic Processes (AE2PPP). The AE2PPP model assures the closest peak-to-peak fit of the calculated two-phase results and observed and reported seasonal statistical data with a minimum number of necessary model parameters. The article emphasises the importance of control over the seasonal worsening and recovery phases of climate processes for projections of climate policies to 2100 relaying on the Technical Summary in Climate Change 2021: The Physical Science Basis, 2021 (Arias et al., 2021) based on climatology and on general considerations denoted as the Shared Socioeconomic Pathways (SSP) (See Appendix A).

# **Accumulation of Effects of Two-Phase Periodic Processes**

The introductory presentation of the AE2PPP model is in the form of causal loop diagrams (Figure 1). The

periodic effects within a  $k^{th}$  period consist of progression phase  $E_P(k)$  in period fraction  $T_P$  and regression phases  $E_R(k)$  in period fraction  $T_R$  (Figure 2).

The joint effect of two successive phases P(k) and R(k) is the result of the continuous accumulation of the progression phase effects  $P(k) = R(k-1) + E_P(k)$  and the regression phase  $R(k) = P(k-1) + E_R(k)$  during  $k = 1, 2, 3, \ldots$  successive periods and can be suitably presented in an algorithmic form (Figure 3). The progression phase is the reinforcing loop (+P) and the regression phase is the balancing loop (-R) both exposed to periodic environmental changes. Their imbalance induces changes in periodic processes (Figures 1 and 2). Plausible environmental feedback affecting the accumulation process may be the F[P(k)] to the progression phase P(k) and the F[R(k)] to the regression phase R(k) (Figure 1).

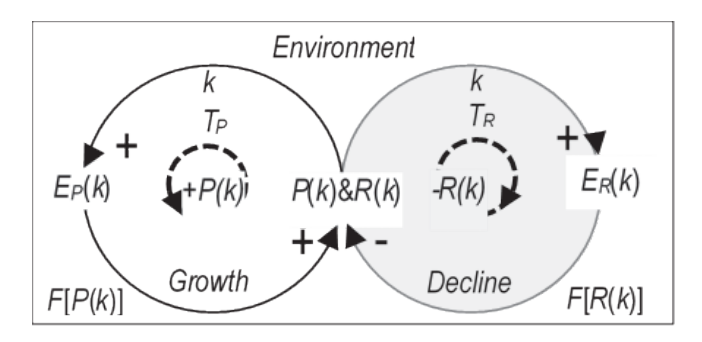


Figure 1: Causal Loop Diagram (CLD) of periodic processes of two alternating phases.

The reinforcing +P and balancing -R loops (Figure 1) are next presented by periodic linearly progressing effect  $E_P(T_P) = pT_P$  and regressing effect  $E_R(T_R) = rT_R$  (Figure 2).

The process recovery rate is  $E_R/E_P$ . The unrecovered effect is  $E_U=E_P$ - $E_R$ . The phase durations  $T_P$  and  $T_R$  are suitably fractions of a unit period  $T_P$ + $T_R=1$ .

The primary (progressive, positive, ascending, growing, increasing, worsening) periodic process phase of linear effect  $E_P(k)$  in time  $T_P$  (Figure 2) starting from the value  $E_{P0}$  at progression rate p for numbers of periods  $k = 1 - T_R$ , 1,  $2 - T_R$ , 2,  $3 - T_R$ , 3... is:

$$E_P(k) = E_{P0} + k \cdot E_P(T_P) = E_{P0} + p \cdot (k - T_R)$$
 (1)

The positive parameter p indicates a linear growth of the progressive effect since the negative parameter r means an increase in the recovery effect in time. The initial recovery rate is  $E_{R0}/E_{P0} =$  and the remaining effect is  $E_{P0}$ - $E_{R0}$  (Figure 2).

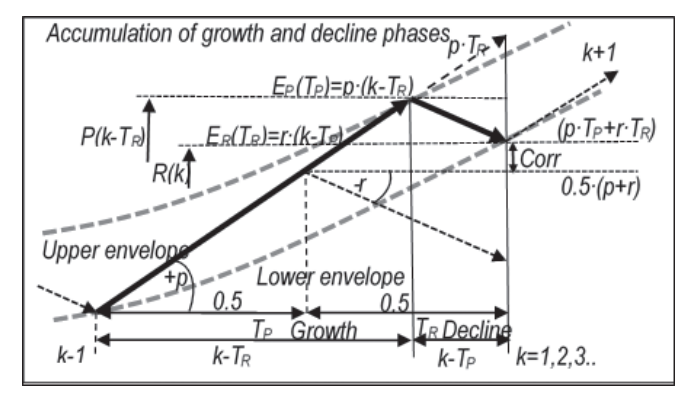


Figure 2: Two-phase periodic process of linear progressing and regressing phases.

The successive (regressive, negative, descending, declining, decreasing, recovering) process phase of linear effect  $E_R(k)$  in time  $T_R$  (Figure 2) starting from value  $E_{R0}$  at regression rate r for numbers of periods k=1, 2, 3... is then as follows:

$$E_{R}(k) = E_{R0} + k \cdot E_{R}(T_{R}) = E_{R0} + r \cdot (k - T_{P})$$
 (2)

The article introduces the numerical algorithm for peak-to-peak accumulation of linear effects of progression and regression phases (1, 2) of periodic processes appropriate for digital processing and presentation (Figure 3).

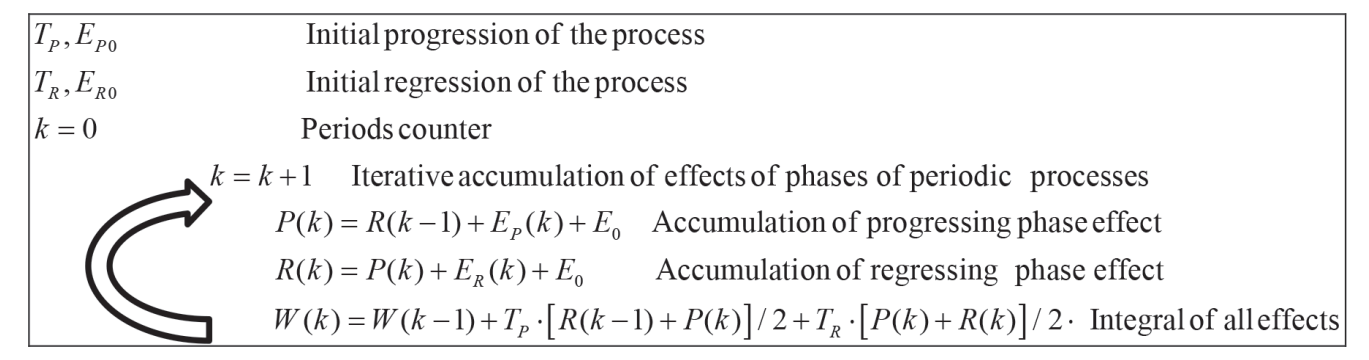


Figure 3: Algorithm for the AE2PPP for accumulation of effects of 2 phase periodic processes.

The summations from peak-to-peak of the linear AE2PPP algorithm (Figure 3) reveal the lower  $E_L(k)$  and upper  $E_U(k)$  envelopes (Figure 4) of the effects as quadratic functions of the periods counter k (1, 2) of the same parameters (see Appendix B), as shown:

$$E_L(k) = \sum_{k} P(k) = A_L \cdot k^2 + B_L \cdot k + C_L$$
 (3)

$$E_{U}(k) = \sum_{k} R(k) = A_{U} \cdot k^{2} + B_{U} \cdot k + C_{U}$$
 (4)

The first derivative of the lower envelope (3) represents the tangent or the sensitivity to changes in the periodic processes:

$$E_T(k) = (A_L + B_L) \cdot k \tag{5}$$

The first step in the application of the AE2PPP algorithm is the identification of the worsening and recovery phases and the peaks of seasonal processes from the observed data. Then the parameters of the AE2PPP model  $(p, r, T_P, T_R, E_{P0}, E_{R0}, E_0)$  can be extracted by application of a general non-linear optimisation procedure until the best fit of calculated peaks to peaks of the observed data, using, for example, the least-squares method (Figure 4). The constraint  $W_{\rm AE2PPP} = W_{\rm o}$  (algorithm Figure 3) and some other if necessary, may contribute to the efficiency and accuracy of numerical calculations. The Generalised Reduced Gradient (GRG) and/or evolutionary methods can be adequate for the numerical solution of the AE2PPP model parameters.

The basic notes on the AE2PPP procedure (Figure 4) are as follows:

 The nonlinearity of the accumulation of linear seasonal effect comes from the acceleration (see APPENDIX B) as follows:

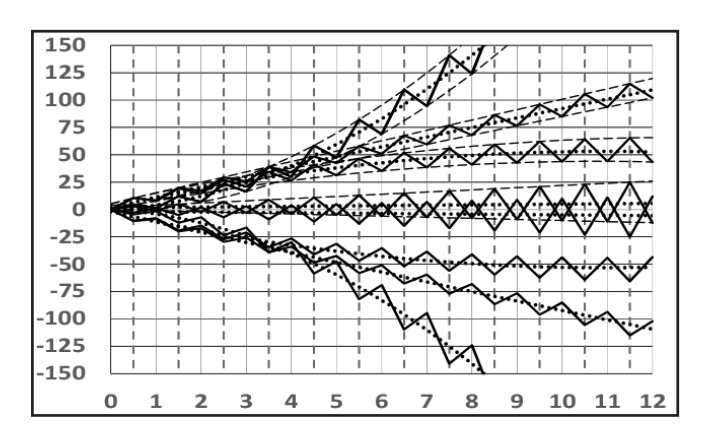


Figure 4: Different models of the AE2PPP (uniform, sublinear, linear, supra-linear and negative).

$$a = p + r \tag{6}$$

- the AE2PPP is uniform for  $E_{P0} + E_{R0} = 0$  and for zero acceleration a = p + r = 0;
- the AE2PPP is linearly ascending for  $E_{P0} + E_{R0} > 0$ , otherwise is descending;
- the AE2PPP is supra-linear (accelerates) for a = (p + r) > 0, otherwise is sublinear (decelerates);

# **Seasonal Atmospheric Carbon Dioxide Concentration**

The procedure of the AE2PPP at the beginning tackles the observed and reported concentration of atmospheric CO<sub>2</sub> (Global Monitoring Laboratory-Earth System Research Laboratory-Mauna Loa Observatory, 2023).

Reported data (1999-2023) (Figures 5-7) show stable annual growth fraction  $T_P = 0.667$  from September to April and recovery fraction  $T_R = 0.333$  from May to August. The starting value in 2000 is  $P_0 = 365$  ppm. The initial periodic growth  $E_{P0} = +8.0$  ppm/ $T_P$  and recovery  $E_{R0} = -6.2$  ppm/ $T_R$ (2) of  $CO_2$  concentration in 2000 are estimated as the mean values of all peak observations from 2014 to 2023. The initial recovery rate is then -6.2/8.0 = -0.775 indicating that 8.0-6.2 = 1.8 ppm/year or 22.5% of the emitted  $CO_2$  remains annually in the atmosphere. The integral of the reported  $CO_2$  rise from 2000 to 2023 is  $W_0 = 9445$  ppmx years.

The solution of the AE2PPP task provides the seasonal growth and recovery rates p = 0.024 and  $r = 0.012 \ ppm/year$  (Figure 5).

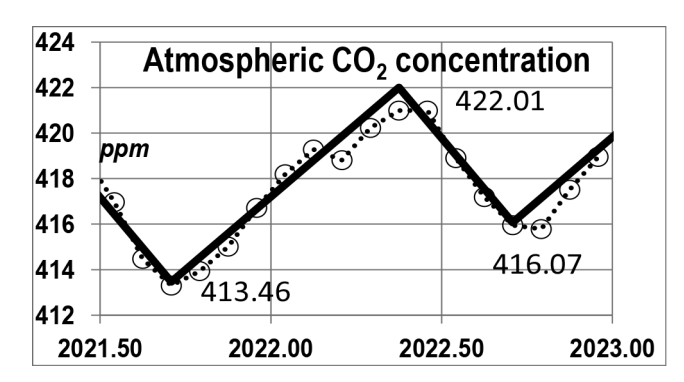


Figure 5: Reported (dotted, circular markers) and the model of AE2PPP of CO<sub>2</sub> concentration.

The positive acceleration rate a = p + r = 0.036  $ppm/year^2$  (6) confirms the supra-linear growth of atmospheric  $CO_2$  concentration relative to the initial growth of 1.83 ppm/year in 2000 (5) (Figure 6) induced both by the increasing seasonal emissions of  $CO_2$  and slowing down the recovery in time.

For the selected *year* is k = (year-1999) and the atmospheric  $CO_2$  concentration in *ppm* is calculated (3, 4) as follows:

$$E_L(year) = 0.018 \cdot k^2 + 1.81 \cdot k + 365$$
 (7)

$$E_U(year) = 0.018 \cdot k^2 + 1.81 \cdot k + 372$$
 (8)

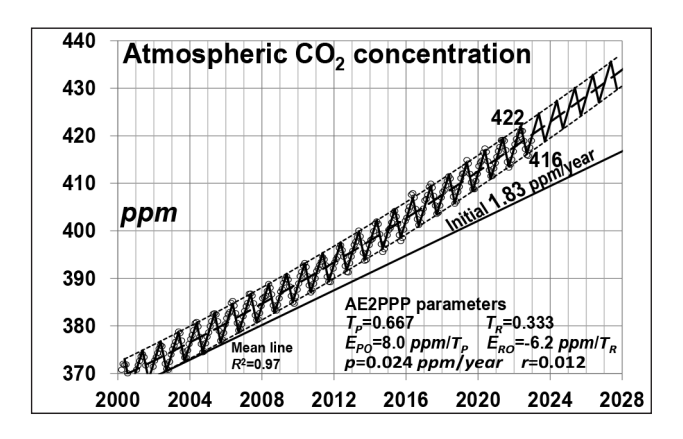


Figure 6: Reported (circular markers) and the AE2PPP model of CO<sub>2</sub> concentration.

The results in 2022 and projections to the end of the century in 2100 (Figures 5-7) are given in the summary (Table 1).

The Shared Socioeconomic Pathways, or SSPs represent five global carbon emissions scenarios relevant to the feedback between plausible climate changes and future technological, demographic, social and economic conditions (APPENDIX A).

The model of AE2PPP next reinterprets the reported SSP scenarios by selected variations of the growth and recovery parameters p and r. The current observations suggest supra-liner growth of  $CO_2$  concentration at 733 ppm to 2100 between the scenarios SSP3-7.0 and SSP2-4.5 (Figure 7).

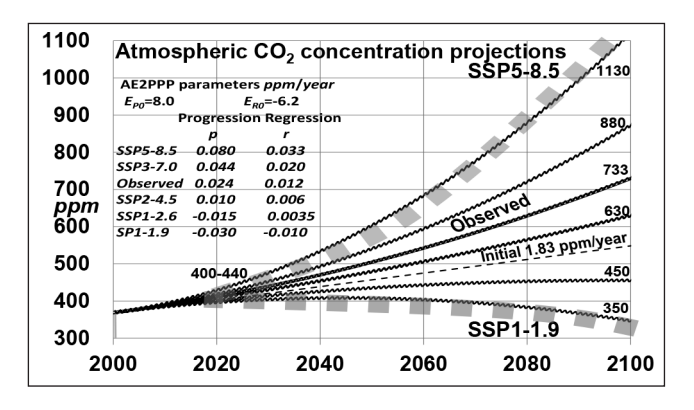


Figure 7: Model of AE2PPP of SSP of CO<sub>2</sub> concentration projections.

The presentation of the SSP scenarios from SSP1-1.9 to SSP5-8.5 (Figure 7) makes it possible to investigate the effects of seasonal growth and recovery of the CO<sub>2</sub> concentration on climate change in time (Figure 8). Reduction of atmospheric CO<sub>2</sub> concentration requires control of annual growth and recovery processes according to favourable SSP scenarios. The delays in protective actions intensify the negative effects of CO<sub>2</sub> concentration growth on climate change (Figure 8).

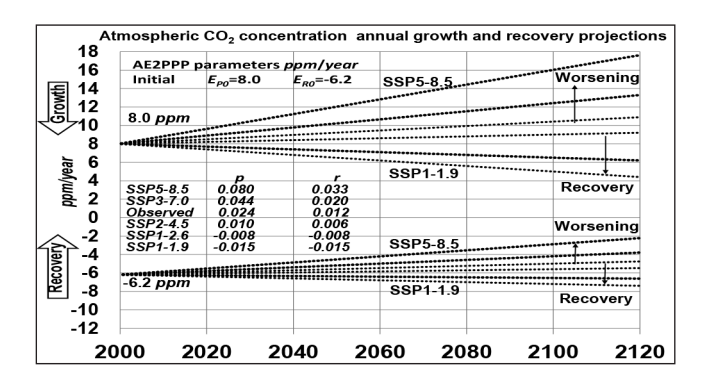


Figure 8: Periodic growth and recovery predictions of atmospheric CO<sub>2</sub> concentration for SSP scenarios.

## Periodic Processes in the Cryosphere

Particularly, the changes in the cryosphere strongly impact global climate change (Liu et al., 2020), and reversely, the seasonal variations in the meteorological conditions seriously impact the balance in the cryosphere (Born, Imhof and Stocker, 2019). The seasonal volume of Antarctica and Greenland ice sheets changes not only under climate effects but also associated with firn air content (Medley et al., 2022). The seasonal energy balance of sea ice is crucial for the Arctic atmosphere-ice-ocean system (Lin et al. 2022). The procedure of the AE2PPP draws the seasonal regularities from the reported peaks of two-phase periodic climate processes simpler than by fitting and time series analysis of climate data (Stark, 2020).

# **Seasonal Ice Mass Losses of the Antarctica Ice Sheet**

Supra-linear ice mass losses of Antarctica and Greenland ice sheets also denoted as ice mass anomalies were observed earlier (Velicogna and Wahr, 2006a; Velicogna and Wahr, 2006b; Velicogna, 2009; Sasgen et al., 2013; Velicogna et al., 2014; Tedesco et al., 2016, 2017, 2019).

The estimated Antarctica ice sheet mass is  $M_{IJ}$ =2.5±0.25 x 10<sup>7</sup> Gt (±10%) (Lythe et al., 2001).

The representative seasonal peaks of observed ice melting and freezing data (2002-2023) indicate constant durations over years of periodic ice melting (losses) of  $T_P$ = 0.5 from July to December and freezing (recovery)  $T_R$ = 0.5 from January to June (Figure 9) (NASA Global Climate Change, Vital Signs of the Planet, 2023). The mean lines of reported and peak data sets coincide. Numerical integration by the trapezium rule of observed data provides the accumulated effects  $W_o$ =-24350 Gtxyeaer.

The solution procedure for this negative problem with the rates of seasonal ice thaw and freeze p=1.0Gt/year and r=-6.7Gt/year. The initial ice mass losses and recovery are  $E_{P0}=-310Gt/T_P$  and  $E_{R0}=230Gt/T_R$ , indicating -80Gt/year or 26% of annual ice mass losses. The starting value is  $P_0=-50Gt$ . Negative acceleration (6) of ice melting a=p+r=-5.7  $Gt/yeaer^2$  (6) indicates supra-linear losses relative to the initial linear growth rate in 2000 of -84 Gt/year (5) (Figure 9b).

For the selected *year* is k=(year-2002) and the Antarctica ice sheet mass losses in Gt are calculated (3, 4) as follows:

$$E_L(year) = -2.84 \cdot k^2 - 87.55 \cdot k - 84.20$$
 (9)

$$E_U(year) = -2.84 \cdot k^2 - 83.68 \cdot k + 226.86$$
 (10)

The results in 2022 and projections to the end of the century in 2100 (Figures 9-10) are given in the summary (Table 1).

The calculated melting-out time of the Antarctica ice sheet according to the AE2PPP model is 2600-3000 years.

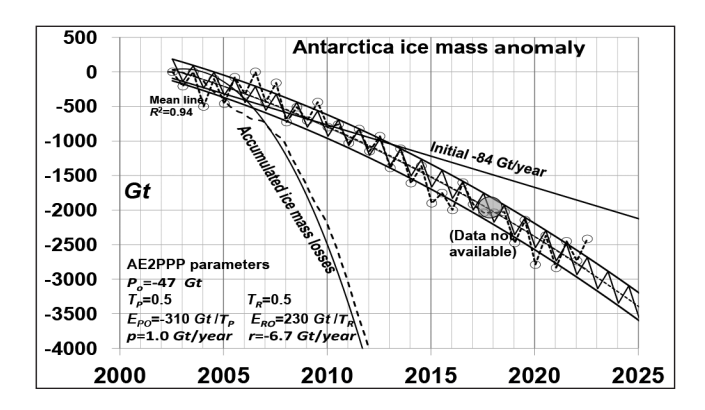


Figure 9: Reported Antarctica ice mass losses (dotted, circular markers) and the model of AE2PPP (black line) (2002-2023).

The article presents projections of the SSP scenarios from SSP1-1.9 to SSP5-8.5 using the AE2PPP for variations of the thaw and freeze parameters *p* and *r* until 2100. The observed losses are between the SSP5-8.5 and SSP3-7.0 scenarios (Figure 10).

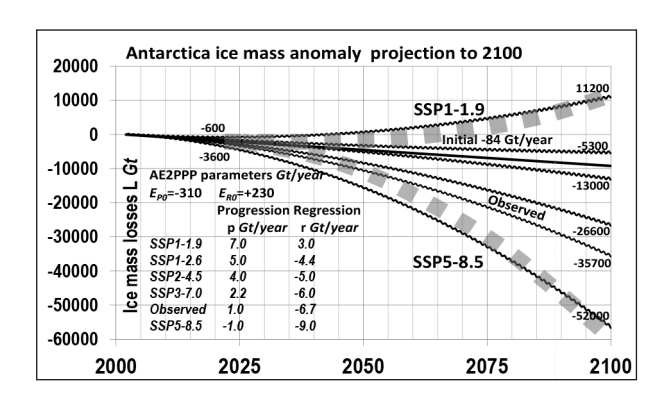


Figure 10: Model of AE2PPP of Antarctica ice sheet losses and SSP projections to 2100.

## **Seasonal Ice Mass Losses of the Greenland Ice Sheet**

The estimated Greenland ice mass is  $M_U$ =2.5±0.20 x 106 Gt (±8%) (Bamber et al., 2001).

The characteristic annual peaks of observed ice melting and freezing data (2002-2023) (Figure 11) indicate seasonal fractions  $T_p$ =0.333 from April to July and  $T_R$ =0.667 from August to March (NASA Global Climate Change, Vital Signs of the Planet, 2023). The mean lines of the two data sets coincide. Numerical integration of observed data provides Wo=-50000 Gtxyeaer.

The AE2PPP problem solution provides the rates of thaw and freezep=-2.06 and r=5.57Gt/year resulting in positive acceleration (6) of ice melting of a=p+r=3.51 Gt/yeaer<sup>2</sup>. The initial periodic ice mass losses  $E_{P0}$ =-426 $Gt/T_P$  and recovery  $E_{R0}$ =117 $Gt/T_R$  indicate annual losses of -310Gt/year (5) or 72% of unrecovered ice. The small positive acceleration suggests a slightly subliner ice mass loss relative to the initial growth (5) in 2002 of -310Gt/year (Figure 11). However, the slowing down of the Greenland ice melting from supra-linear to recent sub-linear occurs after the observations in 2015 (Figure 12).

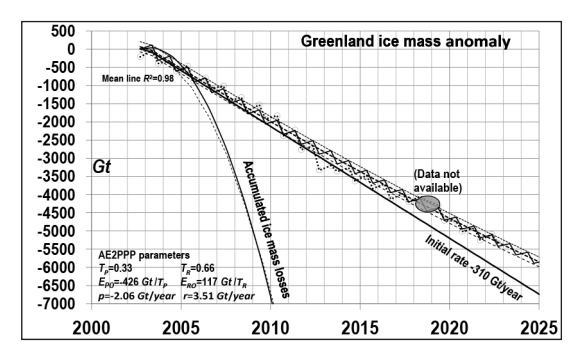


Figure 11: Reported Greenland ice mass losses (dotted, circular markers) and the model of AE2PPP (black line) (2002-2023).

For the selected *year* is k = (year-2003) and the Greenland ice sheet mass losses in Gt is calculated (3, 4) as follows:

$$E_L(year) = 1.75 \cdot k^2 - 309.30 \cdot k + 308.71$$
 (11)

$$E_{II}(year) = 1.75 \cdot k^2 - 308.82 \cdot k + 28.24$$
 (12)

The results of 2022 and projections to the end of the century in 2100 (Figures 11-12) are given in the summary (Table 1).

The article next presents SSP scenarios using the model of the AE2PPP of Greenland ice melting by variations of the thaw and freeze parameters *p* and *r*. The observed losses are between the SSP1-2.6 and SSP1-1.9 scenarios (Figure 12).

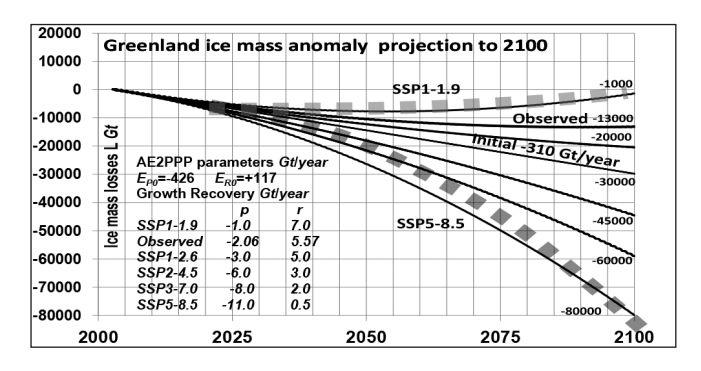


Figure 12: Model of AE2PPP of Greenland ice sheet losses and SSP projections to 2100.

## Seasonal Sea Ice Extent Shrinkage of the Arctic

The annual period of the Arctic sea ice extent consists of the growing (freezing, progressing) phase  $T_P$ =0.5 from October to March and of the shrinkage (thaw, melting, regressing) phase  $T_R$ =0.5 from April to September (Figure 13) (National Snow and Ice Data Center Distributed Active Archive Center, 2023).

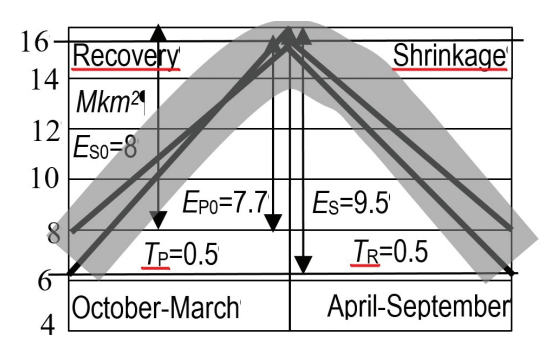


Figure 13: The periods and linearised shrinkage and recovery of Arctic sea ice extent.

The span of the Arctic sea ice is between 6 Mkm<sup>2</sup> in October and 16 Mkm<sup>2</sup> in September (Grosfeld et al., 2016). At the beginning of observations in 1979, the span (A6) was estimated at  $E_c(8)=8Mkm^2$  (Ionita, 2019). Towards the end of observations in 2022, the span (A6) is estimated at  $E_c(51)=9.5 \, Mkm^2$  (Figure 13). The periodic growth and shrinkage of the sea ice extent in 1971 are estimated at  $E_{P0} = 7.7 M km^2 / T_P$  and  $E_{R0} =$ -7.7  $Mkm^2/T_R$  (Figure 14). The parameters of periodic thaw and freeze of Arctic sea ice extent p = +0.0374and  $r = -0.0351 \, Mkm^2/vear$  are determined by fitting the AE2PPP model to the 2<sup>nd</sup> order trendline of the observed annual data in September from 1980 to 2022 (NASA Global Climate Change, Vital Signs of the Planet, 2023) subjected to equality constraint on span in 2022 of  $E_S$  $(51) = 9.5 \ Mkm^2$  (A6). The acceleration is a = p + r = $+0.0023 \ Mkm^2/vear^2$ .

For the selected *year* is k = (year-1971) and the Arctic sea ice freeze and thaw in  $Mkm^2$  is calculated (3, 4) as follows:

$$E_L(year) = -0.001 \cdot k^2 - 0.0163 \cdot k + 7.7$$
 (13)

$$E_U(year) = -0.001 \cdot k^2 - 0.0173 \cdot k + 15.4$$
 (14)

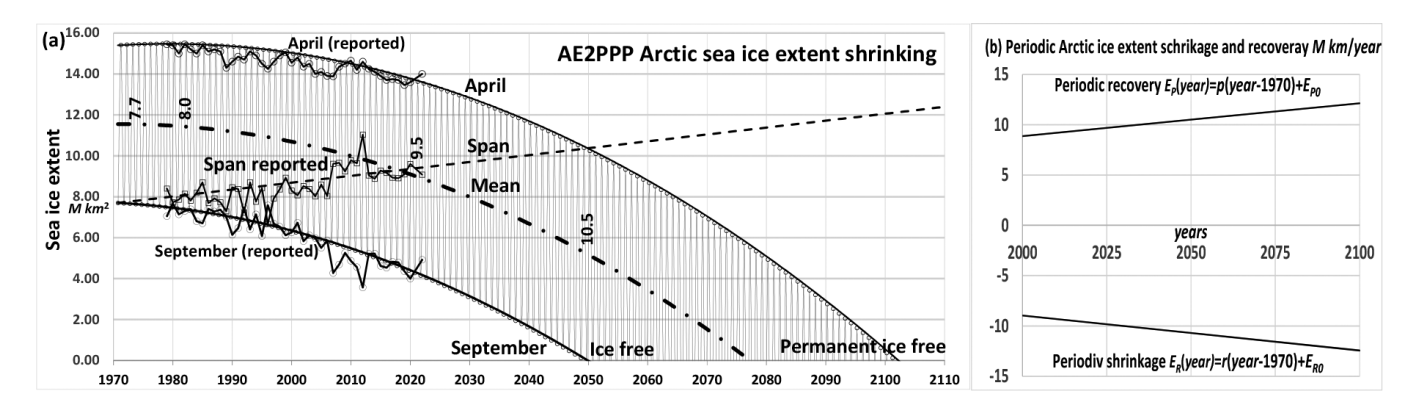


Figure 14: Reported Arctic sea ice extent and AE2PPP model.

In 2022, the shrinkage and the recovery were -9.51 and 9.38 *Mkm*<sup>2</sup>, respectively, indicating a high recovery rate of 0.986%. Notably, even small differences in seasonal thaw and freeze rates induce large periodic process nonlinearity.

The Arctic might start to be ice-free in 2100 (Figure 14a). The AE2PPP shrinkage will be  $E_p(2050) = -10.5 Mkm^2/T_P$  (1) and the recovery  $E_R(2050) = 10.3 Mkm^2/T_R$  (2). The span has been increasing from 1979 to 2050 from 8 to 10.5  $Mkm^2/year$  (Figure 14b).

## 5 Model of the AE2PPP of the seasonal sea level rise

The article next tackles the observed sea level rise (Global Climate Change Vital Signs of the Planet, 2023).

The characteristic seasonal peaks of annual sea level rise and drop are extracted from the observed data (1993-2023) indicating the annual periodic growth and recovery fractions  $T_p = 0.5$  from April to September and  $T_R = 0.5$  from October to Mart (Figure 15). The mean lines of two data sets coincide. The initial periodic growth  $E_{P0} = +15 mm/T_P(1)$  and recovery  $E_{R0}$ =  $-13mm/T_R(2)$  of sea level rise are estimated from the observations in 1993. The initial recovery rate is then 13/15=0.87, indicating that 15-13=2 mm/year or 13%of the annual sea level rise is permanent. The integral of the sea level rise from 1993 to 2023 is  $W_0 = 1310 \text{ mmx}$ *years*. The rates of seasonal growth and recovery are p=0.04 and r=0.04 mm/year. The positive acceleration  $a=0.08 \text{ mm/year}^2$  (6) means supra-linear sea level rise relative to the initial linear growth of 2.07mm/year in 1993 (Figure 15).

For the selected year, k=(year-1993), the Arctic sea level in mm is calculated (3, 4) as follows:

$$E_L(year) = 0.04 \cdot k^2 + 2.02 \cdot k - 2$$
 (15)

$$E_U(year) = 0.04 \cdot k^2 + 2.02 \cdot k + 12$$
 (16)

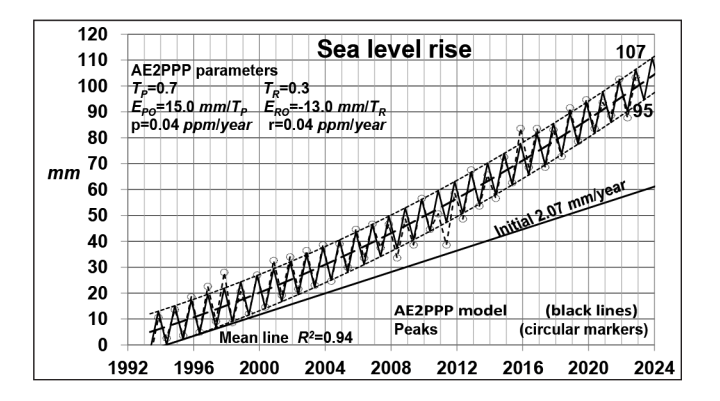


Figure 15: Reported (dotted line, circular markers) and the AE2PPP model of the sea level rise.

The results of observations in 2022 and projections to the end of the century in 2100 are given in the summary (Table 1).

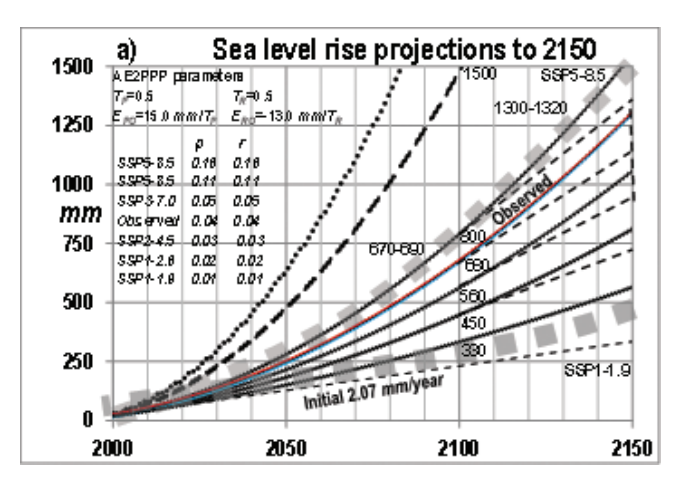
The periodic sea level rise lags behind the  ${\rm CO}_2$  concentration rise at Mauna Loa Observatory for about five months.

The article next presents the feasible SSP scenarios to the end of the century based on the AE2PPP model starting in 2000 by variations of the growth and recovery parameters p and r. The AE2PPP model places the recently reported sea level rise between SSP2-4.5 and SSP3-7.0 scenarios (Figure 16a). Another presentation of the common SSP scenarios makes it possible to investigate the effects of seasonal climate change in the cryosphere on sea level rise and drop (Figure 16b).

Table 1: Summary	/ of	the	results	2000	-2022	-2100
------------------	------	-----	---------	------	-------	-------

Processes	Months	2000				2022				2100				
	Prog/Reg	p	r	а	$E_P$	$E_R$	$E_R/E_P$	P	R	$E_P$	$E_R$	$E_R/E_P$	P	R
CO <sub>2</sub> ppm	9-4;5-8	0.024	0.012	0.036	8.5	-5.9	70%	422	416	10.4	5.0	48%	736	731
Antarctica <i>Gt</i>	7-12;1-6	1.0	-6.7	-5.7	-440	250	56%	-2930	-2680	-970	330	34%	-35900	-35500
Greenland <i>Gt</i>	4-7;8-3	-2.1	5.6	3.5	-320	80	28%	-5180	-5100	120	-90	-75%	-13160	-13250
Arctic Mkm <sup>2</sup>	4-9;10-3	0.037	-0.035	0.002	9.38	-9.51	-0.99	13.54	4.03	10.24	-10.44	0.88%	10.39	0*
Sea level mm	4-9;10-3	0.04	0.04	0.08	16	-12	75%	106	90	19	-9	47%	690	670

<sup>\*</sup>Result for Arctic applies to the year 2050 when it becomes first time ice free in September



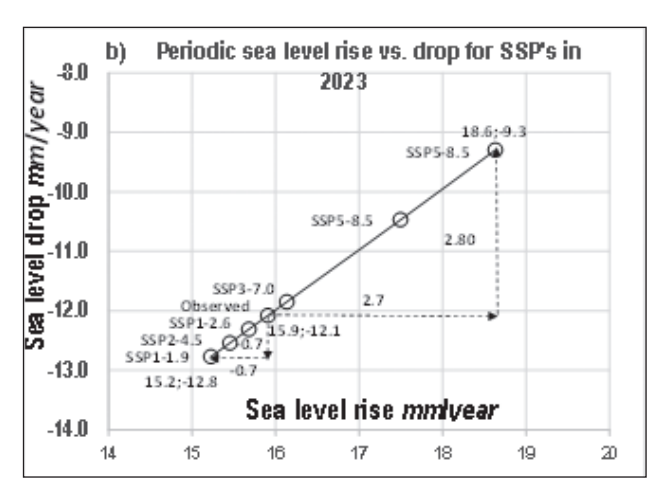


Figure 16: Model of AE2PPP of sea level rise and SSP projections to 2150.

#### Discussion

The observed seasonal climate effects are characterised by the stability of periods and variabilities of intensities in a longer time (Table 1). They also occur in different places and times jointly contributing to global climate change.

The observed highly influential annual atmospheric  $CO_2$  concentration rise period at the Mauna Loa Observatory consists of a growth phase of 8 months from September to April and a recovery phase of 4 months from May to August (Figure 17).

The observed annual Antarctica period consists of a melting phase of 8 months from July to December and a recovery phase of 6 months from January to June which is a 10-month delay after the CO<sub>2</sub> concentration growth and 9 months before the sea level rise. Particularly, the Antarctica ice mass anomaly massively contributes to overall sea level rise (Levermann et al., 2010).

The annual Greenland period consists of a melting phase of 4 months from April to July and a recovery phase of 8 months from August to March which is a 7-month delay after the CO<sub>2</sub> concentration growth and in tempo with the sea level rise. The Greenland ice sheet is another significant contributor to global mean sea-level rise today (Goelzer et al., 2020).

The annual Arctic period consists of a sea ice extent shrinkage phase of 6 months from April to September and a recovery of 6 months from October to March which is a 7-month delay after the  $\mathrm{CO}_2$  concentration and in tempo with the sea level rise. The seasonal energy balance of the Arctic sea ice is crucial for the atmosphere-sea ice-ocean system (Lin, et al. 2022).

The observed annual sea level period consists of a rising phase of 6 months from April to September and a drooping phase of 6 months from October to March which is a 7-month delay after the CO<sub>2</sub> concentration growth (Figure 17).

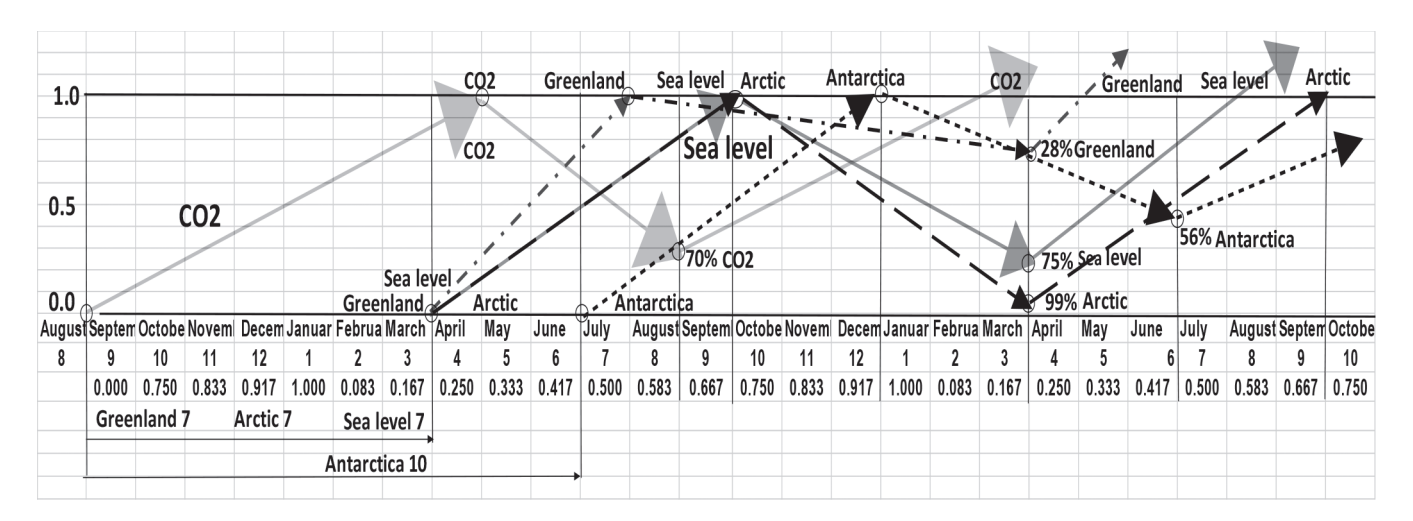


Figure 17: Interactions of the annual CO<sub>2</sub> concentration growth, periodic ice melting and sea level rise in time and space.

There is an empirical lack of physical understanding of the interactions of the ice sheets with the oceans (Goelzer et al., 2020). Nevertheless, the article illustrates the significance of the observed local seasonal climate processes in the cryosphere for the interactions of the sea level rise in *mm* and the seasonal atmospheric CO<sub>2</sub> concentration growth in *ppm* observed at Mauna Loa Observatory (Figure 18) obtained by using the AE2PPP procedure and expressed by the following almost linear relation in time:

$$mm = 1.836 \cdot ppm - 672.48$$
 (17)

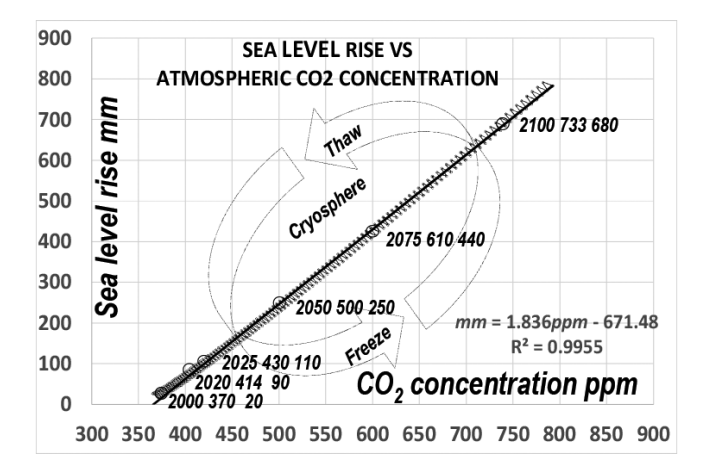


Figure 18: Relations of the sea level rise and the atmospheric CO<sub>2</sub> concentration.

Human influence has warmed the climate at a rate that is unprecedented in at least the last 2000 years (e.g. IPCC, 2021: Summary for Policymakers. *In*: Climate Change 2021: The Physical Science Basis). However, the reported data on global temperature rise are available only on an annual basis (NASA Global Climate Change, Vital Signs of the Planet, 2023) and it is not possible to consider the belonging periodic properties.

## Conclusion

The article finds that the numerical modelling of the accumulation of the effects of two-phase linear periodic climate processes appropriately describes the observed and reported seasonal climate data. Moreover, the seasonal climate processes depend only on two simple sets of parameters: their initial progression and regression intensity and their rates of change in time. Examples in the article based on reported data indicate that the closest peak-to-peak fitting optimisation procedure can identify the plausibly intrinsic periodic regularities of observed seasonal climate variabilities

#### **Nomenclature**

 $T_P$ -period fraction of progression  $E_M$ -mean of effects  $T_R$  -period fraction of regression  $E_s$ -span of effects a -acceleration k -periods counter  $E_0$  -starting effect p -progression rate  $E_{P0}$  -initial progression effect -accumulated progression effects  $E_{R0}$  -initial regression effect r -regression rate  $E_I$ -lower envelope of effects R -accumulated regression effects  $E_{I/}$ upper envelope of effects W-integral of all effects P and R

over a long time. Since the periodic climate processes often dominantly depend on their observable seasonal peaks, the linearity assumption of their periodic two-phase effects suffices applications. The considered seasonal climate processes have stable periods but variable intensities normally at constant rates of changes under observed conditions. The method presented in the article enables control of the necessary reductions of worsening phases and urging of recovery phases of seasonal atmospheric carbon dioxide concentration, land and sea ice melting and sea level rise. This information was useful for long-term future climate scenarios for global temperature rise control and knowledgeable planning of sustainable global climate change policies.

## Acknowledgements

Gratitude belongs to institutions, laboratories, teams, researchers, publishers, and supporting and devoted individuals for making scientific findings and climate data collections publically available for researchers worldwide. The article does not contain AI-generated text.

#### **Funding**

This is a curiosity-driven research and did not receive any grant from funding agencies in the public or commercial sectors.

## **Declaration of competing interest**

The author declares that he has no known competing financial interests or personal relationships that could have appeared to influence the work reported in this paper.

## **Data Availability Statement**

All atmospheric CO<sub>2</sub> concentration data, Antarctica and Greenland ice sheets data as well as the sea level

rise data used during this study are openly available at NASA Global Planet Change, Vital Signs of the Planet: Jet Propulsion Laboratory, California Institute of Technology at https://climate.nasa.gov/\_

All Arctic sea ice data used during this study are openly available at NASA National Snow and Ice Data Center Distributed Active Archive Center are openly available at https://nsidc.org/arcticseaicenews/ and at https://climate.nasa.gov/.

All Shared Socioeconomic Pathways (SSP) scenarios of climate policies projected to 2100 cited by Arias et al. (2021) in the Technical Summary in Climate Change 2021: The Physical Science Basis) used during this study are available at doi:10.1017/9781009157896.002, 2021.

## Appendix A

# **Descriptions of the Shared Socioeconomic Pathways (SSP)**

The work on quantifying one of the five Shared Socioeconomic Pathways (SSPs) was initiated in 2011 by International Institute for Applied System Analysis IIASA (https://iiasa.ac.at/models-tools-data/ssp). The Shared Socioeconomic Pathways, or SSPs represent five global carbon emissions scenarios relevant to the feedback between plausible climate changes and projected future technological, demographic, social and economic conditions from 2015 to 2100. The narratives for scenarios (O'Neill, B. C., et al.) are as follows.

## SSP1: Sustainability (Taking the Green Road)

The world shifts gradually, but pervasively, toward a more sustainable path, emphasizing more inclusive development that respects predicted environmental boundaries. Management of the global commons slowly improves, educational and health investments accelerate the demographic transition, and the emphasis on economic growth shifts toward a broader emphasis on human well-being. Driven by an increasing commitment to achieving development goals, inequality is reduced both across and within countries. Consumption is oriented toward low material growth and lower resource and energy intensity.

## SSP2: Middle of the road

The world follows a path in which social, economic, and technological trends do not shift markedly from historical patterns. Development and income growth proceed unevenly, with some countries making relatively good progress while others fall short of expectations.

Global and national institutions work toward but make slow progress in achieving sustainable development goals. Environmental systems experience degradation, although there are some improvements and overall the intensity of resource and energy use declines. Global population growth is moderate and levels off in the second half of the century. Income inequality persists or improves only slowly and challenges to reducing vulnerability to societal and environmental changes remain.

## SSP3: Regional rivalry (A Rocky Road)

A resurgent nationalism, concerns about competitiveness and security, and regional conflicts push countries to increasingly focus on domestic or, at most, regional issues. Policies shift over time to become increasingly oriented toward national and regional security issues. Countries focus on achieving energy and food security goals within their own regions at the expense of broader-based development. Investments in education and technological development decline. Economic development is slow, consumption is material-intensive, and inequalities persist or worsen over time. Population growth is low in industrialised and high in developing countries. A low international priority for addressing environmental concerns leads to strong environmental degradation in some regions.

## SSP4: Inequality (A Road Divided)

Highly unequal investments in human capital, combined with increasing disparities in economic opportunity and political power, lead to increasing inequalities and stratification both across and within countries. Over time, a gap widens between an internationallyconnected society that contributes to knowledge- and capital-intensive sectors of the global economy, and a fragmented collection of lower-income, poorly educated societies that work in a labour-intensive, low-tech economy. Social cohesion degrades and conflict and unrest become increasingly common. Technology development is high in the high-tech economy and sectors. The globally connected energy sector diversifies, with investments in both carbon-intensive fuels like coal and unconventional oil, but also low-carbon energy sources. Environmental policies focus on local issues around middle and high income areas.

# SSP5: Fossil-Fueled Development (Taking the Highway)

This world places increasing faith in competitive markets, innovation and participatory societies to produce rapid technological progress and development of human capital as the path to sustainable development. Global markets are increasingly integrated. There are also strong investments in health, education, and institutions to enhance human and social capital. At the same time, the push for economic and social development is coupled with the exploitation of abundant fossil fuel resources and the adoption of resource and energy-intensive lifestyles around the world. All these factors lead to rapid growth of the global economy, while the global population peaks and declines in the 21st century. Local environmental problems like air pollution are successfully managed. There is faith in the ability to effectively manage social and ecological systems, including by geo-engineering if necessary.

Following the Technical Summary in Climate Change 2021: The Physical Science Basis, 2021 (Arias et al., 2021), these five scenarios may be presented more succinctly, as follows:

- SSP1-1.9: carbon emissions rapidly decline to net zero by about 2050, and become negative after that
- SSP1-2.6: carbon emissions decline to net zero by about 2075, and become negative after that
- SSP2-4.5: carbon emissions rise slightly, before declining after 2050, but not reaching net zero by 2100
- SSP3-7.0: carbon emissions rise steadily to become double their current amount by 2100
- SSP5-8.5: carbon emissions rise steadily, doubling by 2050 and more than tripling by the end of the century
- The five scenarios feasibility ranking is expressible as follows:
- SSP1-1.9: very ambitious scenario represents the 1.5°C goal of the Paris Agreement
- SSP1-2.6: sustainable development scenario
- SSP2-4.5: intermediate scenario
- SSP3-7.0: regional rivalry scenario
- SSP5-8.5: fossil-fuel based development

## Appendix B

#### The Envelopes of Effects of Periodic Processes

The summations from peak-to-peak of the linear AE2PPP algorithm (Figure 3) reveal the mathematical envelopes of the effects of periodic processes as quadratic functions of the periods counter k based on the same parameters (1, 2).

The lower envelope is the sum of the regressing effects R(k) (2) for  $k=1-T_R$ , 1,  $2-T_R$ , 2,  $3-T_R$ , 3... and for  $E_{I,0}=0$ , as shown:

$$E_{L}(k) = \sum_{k} R(k) = \sum_{k} (E_{P0} + E_{R0}) + \sum_{k} p \cdot (k - T_{R})$$

$$+ \sum_{k} r \cdot (k - T_{P}) + \sum_{k} p \cdot T_{R}$$

$$= \sum_{k} (p + r) \cdot k + \sum_{k} (E_{P0} + E_{R0}) + \sum_{k} rT_{P}$$
(A1)

The correction for different durations of growing and decline phases (Figure 2) (for  $T_P=T_R=0.5$ , Corr=0) is as shown:

$$Corr = (p \cdot T_p + r \cdot T_R) - 0.5 \cdot (p+r)$$
 (A2)

Applying integration instead of summation in (A1), the lower envelope appears as a quadratic function of k defined by coefficients  $A_L$ ,  $B_L$  and  $C_L$  as follows:

$$E_L(k) = \sum_{L} P(k) = A_L \cdot k^2 + B_L \cdot k + C_L$$
 (A3)

$$A_L = (p+r)/2$$
;  $B_L = (E_{P0} + E_{R0}) + r \cdot T_p + Corr$ ,  $C_L = E_{L0} + E_0$ .

The upper envelope is the sum of effects of progressing effects P(k) (1) for k=1, 2, 3... and for  $E_{U0}=P(T_P)-E_{U0}(T_P)$  defined by coefficients  $A_U$ ,  $B_U$  and  $C_U$  as shown:

$$E_U(k) = \sum_k R(k) = A_U \cdot k^2 + B_U \cdot k + C_U$$
 (A4)

$$A_U = (p+r)/2$$
,  $B_U = (E_{P0} + E_{R0}) + p \cdot T_R + Corr$ ,  
 $C_U = E_{U0} + E_0$ 

The first derivative of the lower envelope represents the tangent or the sensitivity to changes in the periodic processes:

$$E_T(k) = (A_I + B_I) \cdot k \tag{A5}$$

Subsequently, the span is the difference between (A3) and (A4) for all k as follows:

$$E_S(k) = [E_U(k) - E_L(k)]$$
  
=  $k \cdot (p \cdot T_R - r \cdot T_P) + (E_{U0} - E_{Lo})$  (A6)

The span is divergent for  $pT_R+rT_P>0$ .

The mean line is simply a combination of (A3) and (A4) as follows:

$$E_M(k) = E_I(k) + E_S(k)/2 = E_U(k) - E_S(k)/2$$
 (A7)

The nonlinearity of periodic processes comes from the second derivative of the AE2PPP as follows:

$$a = 2 \cdot A_L = 2 \cdot A_U = p + r \tag{A8}$$

#### References

- Arias, P.A., Bellouin, E.N., Coppola, E., Jones, R.G., Krinner, G., et al. (eds.). 2021. Cambridge University Press, Cambridge, UK and New York, NY, USA, pp. 33-144. doi:10.1017/9781009157896.002.
- Bamber, J.L., Layberry, R.L. and Gogineni, S.P., 2001. A new ice thickness and bed data set for the Greenland ice sheet 1. Measurement, data reduction, and errors. *Journal of Geophysical Research-Atmospheres*, **106** (**D24**): 33,773-33,780
- Born, A., Imhof, M.A. and Stocker, T.F., 2019. An efficient surface energy-mass balance model for snow and ice. *Cryosphere*, **13(5)**: 1529-1546.
- Contribution of Working Group I to the Sixth Assessment Report of the Intergovernmental Panel on Climate Change. *In:* Masson-Delmotte, V.P., Zhai, A., Pirani, S.L., Connors, C. et al. (eds.). Cambridge University Press, Cambridge, United Kingdom and New York, NY, USA, pp. 3-32, doi:10.1017/9781009157896.001.
- Global Climate Change, Vital Signs of the Planet at https://climate.nasa.gov/(accessed March 2023).
- Global Monitoring Laboratory- Earth System Research Laboratory-Mauna Loa Observatory at https://climate.nasa.gov/ (accessed March 2023).
- Goelzer, H., Nowicki, S., et al., 2020. The future sea-level contribution of the Greenland ice sheet: A multi-model ensemble study of ISMIP6. Cryosphere, **14(9)**: 3071-3096, https://doi.org/10.5194/tc-14-3071-2020.
- Grosfeld, K., Treffeisen, R., Asseng, J., Bartsch, A., et al., 2016. Online sea-ice knowledge and data platform www.meereisportal.de. *Polarforschung, Bremerhaven, Alfred Wegener Institute for Polar and Marine Research & German Society of Polar Research*, **85(2):** 143-155. doi:10.2312/polfor.2016.011, 2016.
- Ionita, M., 2019. September Arctic sea ice minimum prediction a skillful new statistical approach. *Earth Syst. Dynam.*, **19(1):** 189-204. 10.5194/esd-10-189-2019, 2019.
- Jones, F.C., 2016. Cumulative effects assessment: Theoretical underpinnings and big problems. *Environmental Reviews*, **24(2):** 187-204, https://doi.org/10.1139/er-2015-0073
- Levermann, A., Winkelmann, R., Albrecht, T., Goelzer, H., et al., 2020. Projecting Antarctica's contribution to future sea level rise from basal ice shelf melt using linear response functions of 16 ice sheet models (LARMIP-2). *Earth Syst. Dynam.*, **11:** 35-76. https://doi.org/10.5194/esd-11-35-2020.
- Lin, L., Lei, R.B. et al., 2022. Changes in the annual sea ice freeze-thaw cycle in the Arctic Ocean from 2001 to 2018. *Cryosphere*, **16(12)**: 4779-4796.
- Liu, S., Wu, T., Wang, X., Wu, X., Yao, X., Liu, Q., Zhang, Y., Wei, J. and Zhu, X., 2020. Changes in the global cryosphere and their impacts: A review and new perspective. *Sciences in Cold and Arid Regions*, 12(6): 343-354. DOI: 10.3724/SP.J.1226.2020.00343.

- Lythe, M.B. and Vaughan, D.G., 2021. BEDMAP: A new ice thickness and subglacial topographic model of Antarctica. *Journal of Geophysical Research-Solid Earth*, **106(B6)**: 11335-11351. doi: 10.1029/2000JB900449.
- Medley, B., Neumann, T.A., Zwally, H.J., Smith, B.E. and Stevens, C.M., 2022. Simulations of firn processes over the Greenland and Antarctic ice sheets: 1980–2021, *The Cryosphere*, **16**: 3971–4011, https://doi.org/10.5194/tc-16-3971-2022.
- NASA Global Planet Change, Vital Signs of the Planet: Jet Propulsion Laboratory, California Institute of Technology at https://climate.nasa.gov/ (accessed February 2023).
- National Snow and Ice Data Center Distributed Active Archive Center at http://nsidc.org/arcticseaicenews/(March 2023).
- O'Neill, B.C., Kriegler, E., Ebi, K.L., Kemp-Benedict, E., Riahi, K., Rothman, D.S. et al., 2017. The roads ahead: Narratives for shared socioeconomic pathways describing world futures in the 21st century. Global Environmental Change, 42: 169-180. doi:10.1016/j. gloenvcha.2015.01.004.
- Roudgarmi, P., 2018. Cumulative effects assessment (CEA): A review. *Journal of Environmental Assessment Policy and Management*, **20(2)**: 1850008, https://doi.org/10.1142/S1464333218500084.
- Sasgen, I., Konrad, H., Ivins, E.R., Van den Broeke, M.R., Bamber, J.L., Martinec, Z. and Klemann, V., 2013. Antarctic ice-mass balance 2002 to 2011: regional reanalysis of GRACE satellite gravimetry measurements with improved estimate of glacial-isostatic adjustment based on GPS uplift rates. *Cryosphere*, **7(5)**: 1499-1512. doi: 10.5194/tc-7-1499-2013.
- Stark, A., 2020. Using Data Science to Understand Climate Change: Atmospheric CO<sub>2</sub> Levels (Keeling Curve)
   Model Fitting and Time Series Analysis at https://towardsdatascience.com/timeseries-data-science-curve-fitting-pandas-numpy-scipy-b0cd938ecb59 (accessed March 2023).
- Tedesco, M., 2016. Greenland Set Melt Records in 2015 Consistent with 'Arctic Amplification' at http://www.ldeo.columbia.edu/news-events/greenland-set-melt-records-2015-consistent-%E2%80%98arctic-amplification%E2%80%99.
- Tedesco, M., Box, J.E., Cappelen, J., Fausto, R.S., Fettweis, X., Hansen, K., Mote, T., Sasgen, I., Smeets, C.J.P.P., van As, D., van de Wal, R.S.W. and Velicogna, I., 2017. Greenland Ice Sheet. Arctic Report Card: Update for 2017, https://www.arctic.noaa.gov/Report-Card/Report-Card-2017/ArtMID/7798/ArticleID/697/Greenland-Ice-Sheet.
- Tedesco, M., Box, J.E., Cappelen, J., Fausto, R.S., Fettweis, X., Hansen, K., Mote, T., Smeets, C.J.P.P., van As, D., van de Wal, R.S.W. and Wahr, J., 2019. Greenland Ice

- Sheet. http://www.arctic.noaa.gov/reportcard/greenland\_ice\_sheet.html.
- Velicogna, I. and Wahr, J., 2006b. Measurements of time variable gravity shows a large mass loss in Antarctica. *Science*, **311**: 1754-1756. doi: 10.1126/science 11237855.
- Velicogna, I., 2009. Increasing rates of ice mass loss from the Greenland and Antarctic ice sheets revealed by GRACE. *Geophys. Res. Lett.*, 36: L19503. doi: 10.1029/2009GL040222.
- Velicogna, I., Sutterley, T.C. and van den Broeke, M.R., 2014. Regional acceleration in ice mass loss from Greenland and Antarctica using GRACE time-variable gravity data. J. Geophys. Res. Space Physics, 41: 8130-8137. doi:10.1002/2014GL061052.
- Velicogna, I. and Wahr, J., 2016. Acceleration of Greenland ice mass loss in spring 2004. *Nature*, **443**: 329-331. doi:10.1038/nature05168.